Published in Computational and Theoretical Chemistry
https://doi.org/10.1016/j.comptc.2022.113589

Thermochemical and kinetic studies of H-abstraction reaction of benzofurans and benzodioxins by H-atoms

Juan-Carlos Lizardo-Huerta, Sonia Taamalli, Kanika Sood, Laurent Gasnot, Florent Louis, Abderrahman El Bakali and Luc-Sy Tran
Université de Lille, CNRS, UMR 8522 - PC2A - PhysicoChimie des Processus de Combustion et de l'Atmosphère, 59000 Lille, France

Abstract
The thermo-kinetic data of the H-abstraction of benzofurans (benzofuran and dibenzofuran) and benzodioxins (1,4-benzodioxin and dibenzo-p-dioxin) have been obtained by the CCSD(T)-F12/CBS//CAM-B3LYP/6-311++G(d,p) method. Based on the Bonding Dissociation Energies (BDE) we have observed a stabilization effect exerted by the O-atom on the H-atoms located in β-position of it, thereby increasing their BDEs. In line with these BDEs, we have classified the H-atoms into four groups: *group 1*, H-atoms in the benzene ring unaffected by the stabilization effect of the oxygen atom; *group 2*, H-atoms in the benzene ring under the influence of the stabilization effect of the oxygen atom; *group 3*, H-atoms positioned in the dioxin ring and *group 4*, H-atoms located in the furan ring. We have calculated and evaluated the kinetic constants for the H-abstraction reactions for each of these H-atoms thereby deducing the average values for each type of the H-abstracted.

KEYWORDS: *Hydrogen abstraction, OPAHs, UCCSD(T)-F12/CBS, Combustion, Kinetics.*

1. Introduction

Oxygenated polycyclic aromatic hydrocarbons (OPAHs) are compounds that have one or more oxygen atoms bonded to their aromatic ring. They are produced from the same sources as polycyclic aromatic hydrocarbons (PAHs), because they are both products of incomplete combustion of hydrocarbons [1,2] and biofuels [3–5], as well as during biomass combustion [6]. Moreover, OPAHs may also formed through postemission oxidation of PAHs by chemical oxidation reactions [2]. Like PAHs, these compounds are also estimated to be precursors of soot formation, while being more toxic and harmful to human health [7,8].

Amongst recent studies in the literature, we can cite the work of Suzuki *et al*. who have worked on the oxidation of ethylene [9] and toluene [10] using a flow reactor, whereby they identified the formation of benzofuran, dibenzofuran, 9-fluorenone and benzanthrone, and have proposed a sub-mechanism to explain the formation of benzofuran and dibenzofuran based on the theoretical works by Liu *et al*. [11] and Shi *et al*. [12]. The latter study consists of a developed mechanism to explain the formation of some OPAHs (benzofuran and dibenzofuran) via the HACA mechanism [13] from activated phenoxy radicals obtained from the oxidation of benzene. Altarawneh *et al.* [14] studied the reaction of dibenzofuran (DBZF) with O_2 and focused on the low-temperature chemistry of the first O_2 addition on the DBZF radicals. Keita *el al.* [15] found that some OPAHs could decompose to PAHs. The authors

remarked that the oxidation of dibenzofuran could play a crucial role in the formation of naphthalene in a jet-A1 flame.

Chemistry of the formation of some OPAHs from biofuels was investigated in some experimental studies based on the combustion of anisole [16–18]. Anisole decomposes rapidly to form phenoxy and methyl radicals. These phenoxy radicals can act as building blocks and then participate in the formation of benzofuran and dibenzofuran. Several kinetic models have been developed in the literature to explain the combustion mechanisms of anisole [4,17,19,20]. Unfortunately, the chemistry of formation/decomposition of OPAHs has been little explored in these models, despite their increasing significance. A recent work performed by Chen *et al*. [21] demonstrates the chemistry of the formation of a greater numbers of OPAHs during the combustion of anisole in a jet stirred reactor (JSR). They have identified about 40 OPAHs (2 – 3 cycles) out of which only a few OPAHs (like benzofuran or dibenzofuran) have been quantified and were compared with simulations performed using the model proposed by Wagnon *et al*. [17]. The authors have set forth a certain number of new plausible pathways for the formation of OPAHs via calculations of Gibbs free energies which were earlier not included in the model.

On account of their relevance in terms of their toxicity and how they are formed, several studies have been dedicated to the formation/decomposition of small OPAHS (2-3 cycles). As it is highly likely that these small OPAHs are probable precursors of larger OPAHs. The latter may eventually condense to form soot. It can be anticipated that primary OPAHs (2-3 cycles) may gradually contribute to the formation of larger species. We believe that the initial decomposition reactions involve addition reactions on the double bond and/or H-abstraction reactions, both by H or OH free radicals. Thereafter, the formation of reactive cyclic intermediates formed would allow the production of larger or different OPAHs than the ones currently detected, either by the well-known HACA mechanism [13] or other cyclisation reactions [3,22].

Thus, the aim of our project is to study the different decomposition pathways of representative OPAHs. In this paper we are presenting a first part where we consider H-abstraction reactions by the H-atom on two representative OPAHs: benzofuran (BZF, C_8H_6O) and dibenzofuran (DBZF, $C_{12}H_8O$). To complete this section, we have also included other cyclic species such as benzodioxins such as: 1,4-benzodioxin (BZD, $C_8H_6O_2$) and dibenzo-p-dioxin (DBZD, $C_{12}H_8O_2$). Although the latter species have not been identified experimentally so far, we consider them as potential OPAHs that could be formed by the decomposition chemistry of phenol or during the decomposition of dibenzofuran. For this purpose, we have used an accurate extrapolation to the basis set (CBS) where the limit of energies was calculated explicitly with CCSD(T)-F12a methods and cc-pVDZ and cc-pVTZ levels of theory. Reaction rate rules have been be provided, which can be useful for the development of the formation/decomposition of OPAHs in kinetic models.

2. Computational details

2.1 Electronic structure calculations

The geometry optimisations, transition state, intrinsic reaction coordinate (IRC) and associated harmonic vibration frequency calculations were determined with the DFT method CAM-B3LYP/6-311++G(d,p) basis set with Gaussian16 [23]. The frequencies obtained with this method were scaled using a factor of 0.953 [24]. This method was chosen after a benchmark where we found a better agreement between the calculated values and their experimental (or literature) counterparts for the vibrational frequencies and some thermodynamic

properties, as well as a good agreement in the determination of the transition states. A comparison of the IR spectra and the thermodynamic properties calculated via other evaluated methods (B97D3, M06-2X and B2PLYP-D3) along with the reference data (extracted from NIST database [25]) has been presented in the Supplementary Materials (**Figs. S1 - S2** and **Tables S3 - S4**). Single-point energy calculations were performed using the CCSD(T)-F12a approach with the cc-pVTZ basis set with MOLPRO [26] (denoted CCSD(T)-F12a/VTZ). In addition, calculations of the electronic energies obtained with the CCSD(T)-F12a/cc-pVDZ and CCSD(T)-F12a/cc-pVTZ levels were extrapolated to the complete basis set (CBS) limit energy (denoted CCSD(T)-F12/CBS), using Schwenke's generalised formula [27]:

$$E_{cbs} = \{(E_{large} - E_{small})F + E_{small}\} \qquad (1)$$

where the parameter 'F' is dependent on the calculation method. As 'F' is not available for the envisaged calculation method in this work, we decided to determine it by using the procedure described in the work of Hill *et al.* [28] from the reference frozen-core CCSD and triple correlations energy for small molecules containing first and second row atoms (available in that work). Thereby, we have found optimized CBS coefficients (F) of 1.3638 for the extrapolation of CCSD-F12a correlation energies using the 3C(FIX) *Ansatz* and 1.6084 for the extrapolation of the triple contribution to the CCSD(T)-F12a/3C(FIX) correlation energy, with a mean absolute error (MAE) of 0.219 and 0.090 mE_h respectively.

2.2 Rate constant calculations

Rate constants have been calculated based on the canonical transition state theory (TST) [29–31] coupled with statistical thermodynamics to evaluate the partition functions as described by the following expression:

$$k(T) = \kappa\sigma \frac{k_B T}{h} \frac{Q_{TS}(T)}{Q_R(T)} \, exp\left(-\frac{E_0}{RT}\right) \qquad (2)$$

Here; 'κ' is the transmission coefficient and it is computed from the one dimensional asymmetric Eckart potential [32]. 'σ' is the statistical factor and considers external symmetries and optical isomers of the reactants as well as the TS. 'k_B' is Boltzmann's constant, 'h' is Planck's constant, 'T' the temperature and 'E_0' represent the classical barrier height. '$Q_{TS}(T)$' and '$Q_R(T)$' are the total partition functions of the transition state and the reactants, respectively.

Finally, we fitted rate coefficients from eqn (2) over the temperatures range 500 – 2000 K to a three parameter Arrhenius expression:

$$k(T) = AT^n \, exp\left(-\frac{E_a}{RT}\right) \qquad (3)$$

The calculation of the kinetic and thermodynamic parameters, following this methodology, was carried out using the ThermRot software [33]. This software makes it possible to easily retrieve the relevant data from the Gaussian calculation files as well as to calculate the kinetic parameters and thermodynamic data in the form of NASA polynomials.

3. Results and discussion

3.1 Structural properties

The different structures and abstraction sites of the studied species are presented in **Fig. 1a**.,with their respective C-H Bonding Dissociated Energies (BDE) at 298 K. These energies were calculated at CCSD(T)-F12/CBS and CCSD(T)-F12a/VTZ level of theory.

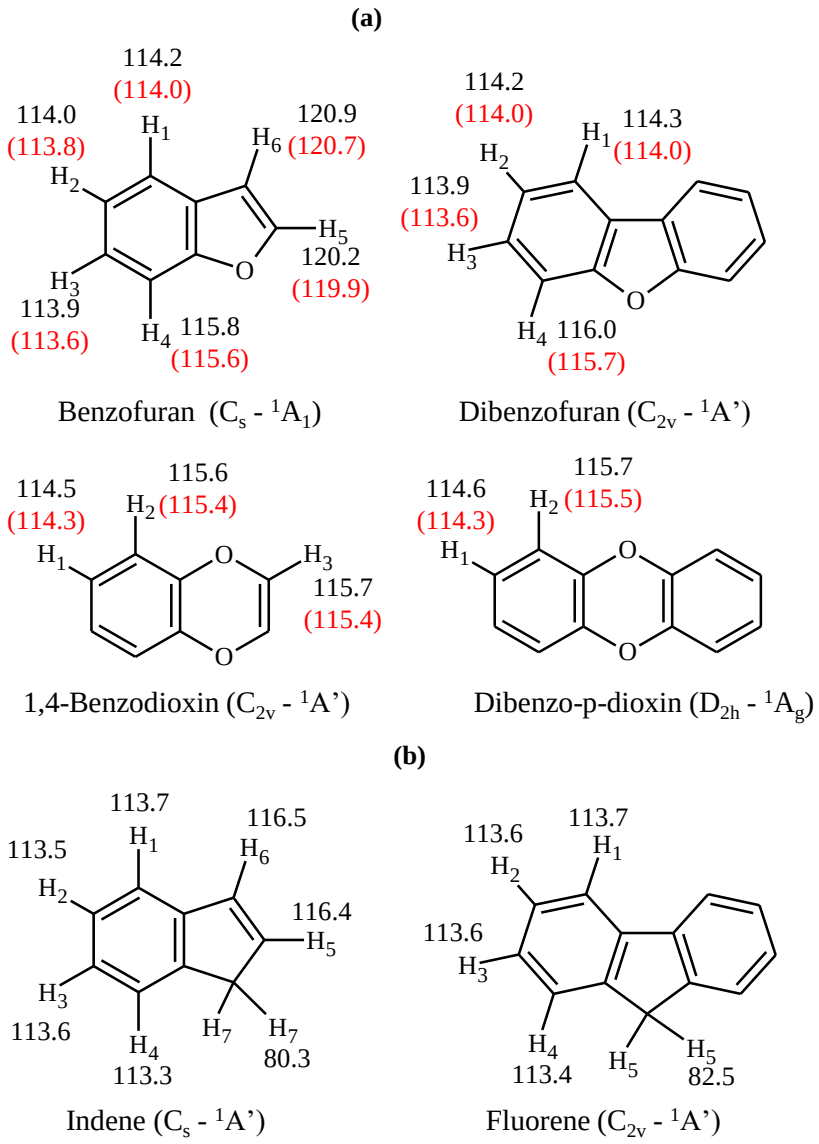

Fig. 1. Structures of: (a) OPAHs studied and, (b) PAHs counterparts of BZF and DBZF (indene and fluorene respectively) with their respective numbered H-abstraction sites and their C-H BDE at 298 K (in kcal mol^{-1}), calculated at CCSD(T)-F12/CBS and CCSD(T)-F12a/VTZ (in bracket).

From the BDE values, it can firstly be observed that the CCSD(T)-F12a/VTZ method slightly underestimates the BDEs (in brackets) as compared to those obtained with the CCSD(T)-F12/CBS method (around 0.3 kcal mol^{-1}).

Secondly, it can be observed that apart from benzofuran (where there are H-atoms bound to the furan ring), the BDEs are all in the range 113.5 - 116.5 kcal mol^{-1}, and close to that of benzene (113.4 kcal mol^{-1} at the same level of theory). Also, with a slight increase in the energy value is observed when the carbon atom bound to the hydrogen is located close to the oxygen atom (around 116 kcal mol^{-1}). The latter is due to the presence of an O-atom, which exerts a stabilization effect on the C-H bond whenever they are placed in a β-position with respect to the O-atom, which is consistent with the calculate relative stability of dibenzofuranyl isomers [14]. This stabilisation is due to a significant overlap of the p-electron orbitals of the O-atom of the furan (in benzofuran and dibenzofuran) or the dioxin (in 1,4-benzodioxin and dibenzo-p-dioxin) ring with the π-electrons of the benzene ring [34]. This effect is responsible for higher

BDEs and consequently the energy barriers for the H-abstraction reactions will increase, as later presented in this work. The difference in the C-H BDEs between those without and with the influence from the stabilization effect of O-atom is close to 2 kcal mol^{-1}. It should however be noted that although the rate constants for the second type will be smaller than for the first type (at least at low temperature). But, as the temperature would increase, the effect of the energy barrier on the rate constant will be less important as the entropic effects would become more dominant.

While the discussions above are based on the molecules themselves, it could be interesting to compare C-H BDEs of BZF and DBZF with those in indene and fluorene (**Fig. 1b**) (PAHs counterparts of BZF and DBZF, respectively), which allow further authentically the effect of the presence on an O-atom. The O-atom is absent in the chemical structure of these analogues and thus, we observed that all the C-H bonds present in the benzene ring have BDEs of the same order and values for H_5 and H_6 are 4 kcal mol^{-1} higher for BZF than indene. This indicates that the presence of the oxygen atom in the chemical structure of OPAHs has a noteworthy effect on the C-H BDE. This consequently implies that an extension of reaction rates of PAHs to an application for OPAHs needs to be precautionary.

If we look closely at the chemical structures of indene and fluorene and their analogous OPAHs, we observe that the oxygen atom is substituted at a crucial point, since the abstraction in indene and fluorene are most favourable at this point (H_7 and H_5 respectively in **Fig. 1b**). This implies that the radical formed during metathesis of BZF and DBZF would lead to the formation of products with a different character than those observed in the analogous cases.

Ultimately, in the process of looking for analogous abstraction sites with the aim of proposing reaction rate rules, we have relied on the C-H BDEs. We expect to fall into 4 groups of kinetic constants: *group 1*, those close to the benzene's C-H BDEs and without the influence of the O-atom (H_1 - H_3 in BZF and DBZF, and H_1 in BZD and DBZD); *group 2*, those bonded to the carbon located in the β-position with respect to the oxygen atom (H_4 in BZF and DBZF, H_2 in BZD and DBZD); *group 3*, those bonded to the carbon located in the dioxin ring (H_3 in BZD) and *group 4*, those in the furan ring (H_5 and H_6 in BZF). The symmetry number of the studied OPAHs, the number of unique H-abstraction sites and the reaction path degeneracy are reported in **Table 1**.

Table 1. Symmetry number, number of unique H-abstraction sites, and the reaction path degeneracy of the studied OPAHs.

OPAHs	Symmetry number	Number of unique sites	Reaction path degeneracy (σ)
Benzofuran	1	6 (1,2,3,4,5,6)	1
Dibenzofuran	2	4 (1,2,3,4)	2
1,4-Benzodioxin	2	3 (1,2,3)	2
Dibenzo-p-dioxin	4	2 (1,2)	4

The cartesian coordinates and vibrational frequencies of all reactants, products, transitions states and molecular complexes relative to the H-abstraction reactions by H-atom for the benzofurans/benzodioxins and optimized at CAM-B3LYP/6-311++G(d,p) level of theory are given in **Tables S5 - S13** of Supplementary Materials.

One of the characteristics observed in the chemical structures obtained for the TS is that they systematically possess the Point Group 'Cs'. All the OPAHs studied in this work have a

planar structure. Following the H-atom abstraction, the remaining unpaired electron will be delocalized in the aromatic cycle, thereby conserving the planar structure in the transition states, the molecular complexes, or in the product. However, in the case of 1,4-benzodioxin, the abstraction of the H_3-atom (H positioned in the dioxin ring) does not follow this rule because the unpaired electron will not delocalize in the ring due to the presence of the two oxygen atoms. Due to this, the structure would reorient itself to form a kind of semi-chair structure, where its Point-group will become 'C1'.

For all studied transition states, the ratio (L = δr(H-C)/ δr(H-H)) [35] between the elongated values of the C-H bond and the H-H bond is determined to identify the principle changes in the structural properties of the transition state. **Table 2** presents the elongated values of the r(H-H) bond length, the r(H-C) bond length, the bond angle θ(HCC), and the ratio L for the H-abstraction reaction of dibenzofuran by H-atom.

Table 2. Elongated values of the r(H-H) and r(H-C) bond lengths, the bond angle θ(HCC) and the ratio L for the H-abstraction reaction by H-atom from dibenzofuran. Distances are given in angstroms and bond angles in degrees. MCR: Pre-reactive molecular complex and MCP: Post-reactive molecular complex. The number after de label correspond to the numbered H-abstraction sites in **Fig. 1**.

H + DBZF	r(H-H) Å	r(H-C) Å	θ(HCC) °	*L*
MCR1	2.852	1.083	162.5	
TS1	0.842	1.513	178.0	*4.48*
MCP1	0.747	2.993	174.6	
MCR2	2.924	1.083	124.8	
TS2	0.839	1.518	179.8	*4.68*
MCP2	0.748	2.938	160.0	
MCR3	2.925	1.083	125.2	
TS3	0.841	1.512	179.8	*4.52*
MCP3	0.748	2.950	162.6	
MCR4	2.936	1.082	123.3	
TS4	0.831	1.537	177.4	*5.35*
MCP4	0.747	2.980	154.4	

Regarding DBZF, the ratio 'L' is quite similar for the transition states from all abstraction sites corresponding to *group 1* (L ranging from about 4.48 to 4.68) while it is higher for the TS corresponding to *group 2* (TS4). The corresponding values of other species are given in **Table S14** (Supplementary Materials), where all L values show that the transition states are product-like because 'L' > 1. In general, we have found that when H-abstraction is performed on an H-atom located in a 6-membered cycle, L values are the lowest and it increases when the C-atom is located closer to the O-atom. Also, when H-abstraction is performed on a hydrogen atom located in a 5-membered cycle (furan ring), the 'L' value is much higher (between 8 and 8.5).

If we take a closer look at the structural properties of the pre-reactive complexes, we realise that the binding energies are in general lower than 0.1 kcal mol^{-1}, these small values are consistent with the lack of change of the C-H bond distances between the reactants (1.083 Å) and the MCRs (**Tables 2** and **S14**). As a result of these small binding energies, the MCRs do not significantly lower the reaction barriers. Therefore, we consider that the MCRs can be neglected in the calculation of the rate constants.

3.2 Energy barriers and reaction energies

Single-point energy calculations were effectuated using the composite method CCSD(T)-F12/CBS based on the geometries and frequencies obtained from the CAM-B3LYP/6-311++G(d,p) level of theory. We have found that the level CCSD(T)-F12/CBS is a good and very well stablished method for developing potential energy profiles [27,28,36] and in our opinion it is the first time that it is used in the framework of OPAHs with an important molecular size (up to $C_{12}H_8O_2$ - DBZD), with an affordable computational cost.

In **Table 3** we present the values of energy barriers at 0K including the ZPE (E_0), standard reaction energies ($\Delta_r H°_{298K}$) and standard Gibbs free energies ($\Delta_r G°_{298K}$), for all H-abstraction reactions obtained using the CCSD(T)-F12/CBS//CAM-B3LYP/6-311++G(d,p) level of theory. The DFT method CAM-B3LYP has recently been successfully applied to the study of PAHs [37,38]. The calculated BDE at 298 K and the barrier heights at 0 K of the different H-abstraction reaction of studied OPAHs using the CAM-B3LYP/6-311++G(d,p) level of theory are also available in **Table S15** in the Supplementary Materials. In **Table 3** we also present the average values for the same type of H-abstracted atom (*group 1* to *4*). Concerning the H-abstraction sites in *group 3* (only one case, H_3 in BZD), we have included the H-abstraction of 1,4-Benzodioxin.

From these values we can observe that the energy barriers vary according to the nature of the H-abstracted, with *group 1* H (H-benzene type) being the most favourable from an energetic point of view, followed by *group 2* (C-H in the β-position of the oxygen atom), followed by *group 3* (H positioned in the dioxin ring) and finally, *group 4* (H positioned in the furan ring) being the least favourable. The standard enthalpies of reaction are all positive, indicating that at standard conditions (298.15 K), the decomposition processes studied are all endothermic. Similar behaviour has been reported in the case of PAHs [39].

In the case of standard Gibbs free energies, the fact that these values are positive indicates that the H-abstraction processes studied in the framework of the decomposition of OPAHs are non-spontaneous at 298.15 K (standard conditions).

In order to identify at which temperature, the abstraction processes become spontaneous for the different OPAHs studied, we calculated the inversion temperatures (Gibs free energy equal to zero). From the values presented in **Table S16** in the Supplementary Materials, we firstly remarked that there is a clear difference when moving from one group to another group of hydrogens. H-abstractions using *groups 1* and *2* constitute very favourable processes under flame conditions, in contrast to H-abstractions using *groups 3* and *4*. Secondly, on comparing the same group of hydrogens, we observed that the inversion temperature decreases as the number of cycles in the molecule increases. In parallel, on comparing molecules with the same number of cycles but different numbers of O-atoms in their structure (BZF with BZD and DBZF with DBZD), we have noticed that the inversion temperature decreases as the number of O-atoms increase.

These last points are interesting to underline, as it has been shown that the H-abstraction processes do not depend on the ring size and the fact that the Gibbs free energies have a noticeable difference when increasing the number of rings or the number of O-atoms would imply that the latter has a more pronounced effect on the thermodynamic properties than on the kinetic constants. This could also indirectly explain why OPAHs form and decompose more rapidly under flame conditions when compared to PAHs (**Fig. S17** in the Supplementary Materials).

Table 3. Calculated CCSD(T)-F12/CBS//CAM-B3LYP/6-311++G(d,p) barrier heights at 0 K including the ZPE (E_0), reaction energies ($\Delta_r H°_{298K}$) and the standard Gibbs free reaction energies ($\Delta_r G°_{298K}$) of the different abstraction reactions of studied species (in kcal mol^{-1}). *STD: Standard Deviation

H-site (group)	E_0	$\Delta_r H°_{298K}$	$\Delta_r G°_{298K}$
Benzofuran (BZF)			
H_1 (g1)	16.16	9.49	8.01
H_2 (g1)	15.83	9.29	7.82
H_3 (g1)	15.77	9.15	7.67
H_4 (g2)	17.34	11.08	9.59
H_5 (g4)	21.14	15.48	14.00
H_6 (g4)	21.09	16.20	14.73
Dibenzofuran (DBZF)			
H_1 (g1)	16.04	9.54	7.65
H_2 (g1)	15.97	9.50	7.61
H_3 (g1)	15.76	9.13	7.24
H_4 (g2)	17.41	11.24	9.33
1,4-Benzodioxin (BZD)			
H_1 (g1)	16.23	9.78	7.83
H_2 (g2)	17.03	10.91	9.02
H_3 (g3)	18.67	10.93	9.67
Dibenzo-p-dioxin (DBZD)			
H_1 (g1)	16.25	9.85	7.33
H_2 (g2)	17.07	10.97	8.69
1,4-Dioxin			
H_1 (g3)	18.25	9.92	8.78
Average values (STD*)			
Group 1 (g1)	*16.0 (0.201)*	*9.6 (0.266)*	*7.6 (0.257)*
Group 2 (g2)	*17.2 (0.191)*	*11.1 (0.145)*	*9.2 (0.389)*
Group 3 (g3)	*18.5 (0.297)*	*10.4 (0.714)*	*9.2 (0.629)*
Group 4 (g4)	*21.1 (0.035)*	*15.8 (0.509)*	*14.4 (0.516)*

3.3 Kinetic parameters

Previously, we had observed that the energy barriers were slightly lowered when we used the CBS basis extrapolation on the CCSD(T)-F12a/cc-PV(D+T)Z level of theory. Therefore, we wanted to see the influence of this decrease on the kinetic constants. Thus, we present in **Fig. 2** the case of benzofuran and dibenzofuran. From this figure, we can see that the effect is almost negligible, with a factor of 1.1 at 1000K and 1 at 2000 K. Similar behaviour was found for the other OPAHs studied in this work. Following this, all kinetic constants for the concerned species were determined from the results of the electronic structure calculations obtained via CCSD(T)-F12/CBS method.

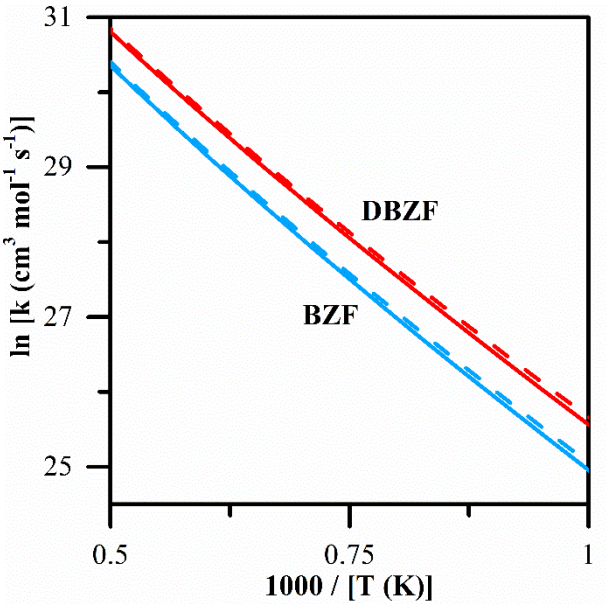

Fig. 2. Comparison of the effect of CCSD(T)-F12/CBS over the total kinetic constants of the H-abstraction in benzofuran (BZF) and dibenzofuran (DBZF). Solid lines, CCSD(T)-F12a/cc-pVTZ and dash lines, CCSD(T)-F12/CBS.

In order to select an appropriate temperature range for comparing the kinetic constants of the H-abstractions at different sites in OPAHs, we identified the temperature zones where the studied OPAHs are formed and consumed. For this purpose, we have carried out simulations of an atmospheric laminar premixed fuel-rich flame of anisole/methane mixture [equivalence ratio of 1.82; gas-phase flow rates (nL/min): methane: 1.7, anisole: 0.2, oxygen: 2.8, nitrogen: 7.4] using the high-temperature mechanism of anisole proposed by the CRECK modelling group [19]. Fuel-rich flame conditions were used in this modelling because it offers the advantage to operate close to aromatic and soot formation conditions. Moreover, this flame type makes it easy to follow the evolution of the concentration of species, including PAHs and OPAHs. Anisole was chosen because it has been recognized as a surrogate for lignin-based biofuels, which is owning to its suitable properties, for instance, its high-octane number and a superior net heating value (33.19 vs 21.3 MJ/L for ethanol). Besides, on account of its weak O-CH_3 bond, anisole is an exemplary and ideal precursor to investigate and understand the chemistry of phenoxy and cyclopentadienyl radicals [40], which are important precursors of PAHs and OPAHs [41].

We used the module "Premixed Laminar Burner-Stabilized Stagnation Flame" with Solve Gas Energy Equation of CHEMKIN Pro [42] for which the results are presented in **Fig. S17** in the Supplementary Materials. These results reveal that the studied OPAHs (BZF and DBZF) start to form at ~800 K with a peak mole fraction at around 1200 K, while their analogous PAHs (indene and fluorene) form a little later (~1000 K) with a maximum peak around 1500 K. This trend where OPAHs are formed and decomposed before PAHs was also observed by Suzuki *et al.* in their oxidation study of non-oxygenated hydrocarbons like ethylene [9] and toluene [10] using a flow reactor.

The kinetic parameters for the H-abstraction reactions calculated for all the studied OPAHs in this work, in the range of temperature of 500 to 2000 K, are presented in **Table 4**. The rate constants at each temperature and the reverse kinetic parameters for each site and OPAH are also available in **Tables S18** and **S19** respectively, in the Supplementary Materials. In **Table 4** we also presented the kinetic constants and branching ratios at 1200 K (approximate area of the peak maximum). From these values, we observed that the ratio

between the H-abstraction of H-atoms of *group 1* and *2* at 1200 K is less than 2. This means that abstractions from *group 1* sites is not significantly faster than abstraction from *group 2* sites. Moreover, under this condition, the available energy is so high that both routes remain equally favourable. However, it should be noted that although the stabilization effect of the O-atom does not play a predominant role in the metathesis processes, nevertheless, its role in other processes such as addition on double bonds is yet to be verified.

On the other hand, with regard to the abstraction of hydrogen atoms from *group 3* (BZD), the presence of two oxygen atoms amplifies the stabilization effect, which will lead to a more significant decrease in the kinetic constants (approximately 3 times lower than for *group 1*). Finally, the kinetic constants for *group 4* (C-H in the furan ring) are the least important with a kinetic constant value which is ~5 times lower than that of *group 1*.

Table 4. Kinetic constants (k) for a temperatures range of 500 to 2000 K and branching ratio at 1200 K (R) for H-abstraction of benzofurans and benzodioxins by H-atom (values per transferable H-atom) computed at CCSD(T)-F12/CBS level of theory. Units are in cm, mol, s and cal.

H-type	$k = A\,T^n \exp(-E_a/RT)$			k_{1200K}	R_{1200K} (%)
	A	n	E_a		
Benzofuran					
H_1 (g1)	9.36×10^{6}	2.16	14600	9.18×10^{10}	23
H_2 (g1)	8.74×10^{6}	2.17	14310	10.4×10^{10}	25
H_3 (g1)	8.06×10^{6}	2.18	14240	10.6×10^{10}	26
H_4 (g2)	1.64×10^{7}	2.11	15960	6.38×10^{10}	16
H_5 (g4)	4.71×10^{7}	2.05	20160	2.06×10^{10}	5
H_6 (g4)	8.83×10^{7}	1.96	20220	2.00×10^{10}	5
Dibenzofuran					
H_1 (g1)	8.52×10^{6}	2.16	14460	8.88×10^{10}	25
H_2 (g1)	9.25×10^{6}	2.16	14470	9.59×10^{10}	28
H_3 (g1)	7.58×10^{6}	2.19	14210	10.8×10^{10}	30
H_4 (g2)	1.72×10^{7}	2.10	16060	5.98×10^{10}	17
1,4-benzodioxin					
H_1 (g1)	1.08×10^{7}	2.17	14770	10.6×10^{10}	50
H_2 (g2)	1.58×10^{7}	2.12	15680	7.42×10^{10}	35
H_3 (g3)	7.66×10^{6}	2.17	16930	3.04×10^{10}	15
Dibenzo-p-dioxin					
H_1 (g1)	1.33×10^{7}	2.17	14800	12.9×10^{10}	64
H_2 (g2)	1.61×10^{7}	2.11	15730	6.90×10^{10}	36
Average values (per abstracted H-atom)					
Group 1	*8.03×10^{6}*	*2.19*	*14440*	*10.4×10^{10}*	
Group 2	*1.51×10^{7}*	*2.12*	*15820*	*6.69×10^{10}*	
Group 3	*7.66×10^{6}*	*2.17*	*16930*	*3.04×10^{10}*	
Group 4	*6.45×10^{7}*	*2.01*	*20190*	*2.10×10^{10}*	

For the H-abstraction reactions from benzofurans and benzodioxins, we recommend using kinetic constants obtained in this work, which depend on the nature of the H-abstracted (presented in **Table 4)**. We also presented the averaged values for each type of H-abstracted (*group 1* to *4*) in this table; the maximum error found after comparing the kinetic constants obtained for each species with the average values of each group is approximately 14, 13, 7 and 3 % for groups 1 to 4 respectively. It should also be noted that these kinetic constants are per abstracted H-atom. In the same way, thermochemical data (used in the Chemkin software)

for benzofurans, benzodioxins and their respective H-abstracted products are presented in the **Table S20** in the Supplementary Materials as NASA polynomials

In order to validate the kinetic constants calculated in this work we wanted to compare them to those presented in the literature. Unfortunately, there is no data available for the species concerned. However, as mentioned before, the hydrogen atoms corresponding to *group 1* are close to benzene, for which experimental data exists in the literature. Among the experimental results, Giri *et al*. [43] proposed kinetic constants from shock tube experiments for a temperature range between 1200 and 1350 K for a pressure of 1.3 and 4.3 bar. While Kieffer *et al*. [44] proposed kinetic constants using the shock tube, for temperatures between 1900 and 2200 K. On the other hand, Baulch *et al.* [45] extrapolated kinetic constants for a larger temperature range (500 to 2000 K) based on experimental results from the equilibrium constants and a least squares fit of the shock tube data for the reverse H-abstraction reaction obtained by Heckmann *et al.* [46] in a range of 1050 to 1450 K; and from the data obtained by Park *et al.* [47] using a pyrolysis/Fourier transform infrared spectrometry (P/FTIRS) in the temperature range of 548-607 K and by pulsed-laser photolysis/mass spectrometry (PLP/MS) in the temperature range of 701-1017 K.

According to the simulation results presented in **Fig. S17**, the range of interest for the representative OPAHs (BZF and DBZF) is between about 1000 and 1400 K (formation, maximum peak and onset of decomposition). We present in **Fig. 3** a comparison (by site) of the experimental data proposed by Giri *et al*. [43] for two pressures and their respective uncertainties (~40 %); with the kinetic rates obtained in this work. Values for benzene (dash dotted) have been determined using the computational approach described in **Section 2**, and the average rate constants (solid line) for the H-abstraction of the benzene type H's (*group 1*) obtained in this work have been presented together. From this figure, we can see that in general the values obtained in this work are in good agreement for the evaluated range of temperature.

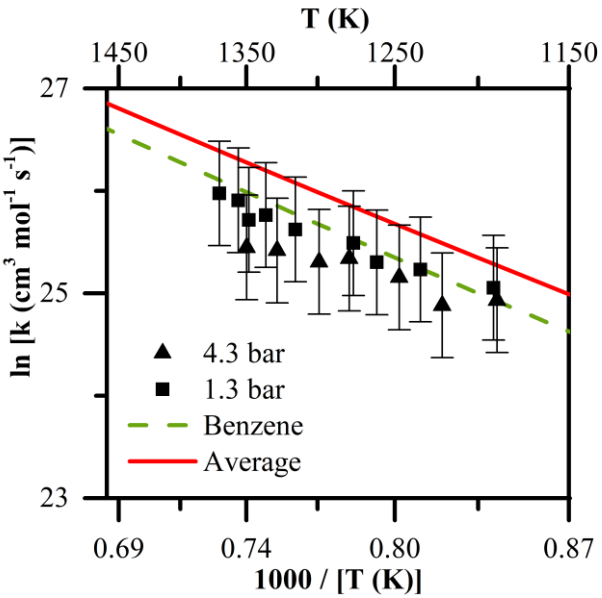

Fig. 3. Experimental (symbols) from literature (Ref. [43]) and calculated in this work (dash doted) rate constants for H-abstraction reaction of benzene by H-atoms; compared to average rate constants (solid line) for H-abstraction of H-benzene type (*group 1*) calculated in this work (rate constants are per site).

4 Conclusion

In this work, we have studied the H-abstractions reaction of some OPAHs (two benzofurans and two benzodioxins) by H-atoms in a systematic way. We identified the CAM-B3LYP/6-311++G(d,p) method as the most suitable for OPAHs for geometry optimisation and frequency calculations. For the limit energy calculations, we opted for the CCSD(T)-F12/CBS composite method with a basis extrapolation of the cc-pVDZ and cc-pVTZ levels of theory from the Schwenke's generalised formula ($E_{cbs} = \{(E_{large} - E_{small})F + E_{small}\}$), where the parameter 'F' determined in this work was derived using a method from the literature.

With respect to the BDEs of the C-Hs bonds, we classified the possible H-abstraction sites into 4 groups: *group 1*, H-atoms in the benzene ring without the stabilization effect of the oxygen atom; *group 2*, H-atoms in the benzene ring with the stabilization effect of the oxygen atom (in β positions according to the oxygen atom); *group 3*, H-atoms positioned in the dioxin ring and *group 4*, H-atoms in the furan ring. The average energy barrier at 0 K of 16.0, 17.2, 18.5 and 21.5 kcal mol^{-1} respectively clearly depends on the type of group. We also found that energy barriers and the enthalpies of reaction do not increase significantly with increasing temperature, which is contrarily not the case for the Gibbs free energies, as it depends more on entropic effects. *Groups 1* and *2* are the most favourable for the purpose with increasing temperature at the expense of *groups 3* and *4* which are non-spontaneous.

The kinetic constants follow the same behaviour of the energy barriers. From the different individual results, we were able to establish averages for each group of hydrogens, as we found that there is no clear effect of the number of cycles due to the close energy barriers for each group. However, we noted a clear effect on the kinetic constants comprising a five-membered ring (*group 4*) being the least favourable; and a rather mixed effect for the abstraction of benzene-type H atoms (*group 1* and *2*), where we found that the stabilization character of the O-atom has an effect on the kinetic constants at lower temperatures and that as we move to flame conditions this effect becomes less important. The magnitude of the difference between these two groups remains rather within the uncertainties of the calculation methodology. Finally, we recommend the use of average kinetic constants for each type of H-atoms in the development of detailed kinetic models in the formation/decomposition of OPAHs.

5 Perspectives

In order to improve the understanding of the different decomposition/formation pathways of OPAHs, we will continue with:

- the study of H-abstraction reactions of OPAHs presented in this article, via the OH and CH_3 radicals. The latter radical is abundant in fuel-rich oxidation of hydrocarbons or biofuels;
- the study of addition reactions on the double bond of cyclic rings via the H and OH radicals;
- the same studies proposed above will be also considered for OPAHs with different functional groups such as the family of quinones or fluorenones;
- evaluate and compare the overall decomposition rate of the PAH/OPAHs dual system.

ORCID

Juan-Carlos Lizardo-Huerta: 0000-0002-1683-3109
Sonia Taamalli: 0000-0002-6200-7115
Laurent Gasnot: 0000-0001-7769-2509
Florent Louis: 0000-0002-9533-557X
Abderrahman El Bakali: 0000-0002-2977-7353
Luc-Sy Tran: 0000-0002-0828-7048

Conflict of interest

There are no conflicts to declare.

Acknowledgments

This work was supported by the I-SITE ULNE through the “Biofuel-Soot” project (R-JEUNES-19-010-TRAN). High performance computing resources were provided by the Centre de Resources Informatiques (CRI) of the University of Lille and IDRIS under the allocation 2020-101578 made by GENCI. We appreciated the support from the French ANR agency Contract No. ANR-11-LABX-0005 “Chemical and Physical Properties of the Atmosphere” (CAPPA). The authors thank the Région Hauts-de-France, and the Ministère de l’Enseignement Supérieur et de la Recherche (CPER Climibio), and the European Fund for Regional Economic Development for their support.

Appendix A. Supplementary Materials

Supplementary data for this article can be found online at

References

[1] C.P. West, A.P.S. Hettiyadura, A. Darmody, G. Mahamuni, J. Davis, I. Novosselov, A. Laskin, Molecular Composition and the Optical Properties of Brown Carbon Generated by the Ethane Flame, ACS Earth Space Chem. 4 (2020) 1090–1103. https://doi.org/10.1021/acsearthspacechem.0c00095.

[2] K.O. Johansson, T. Dillstrom, M. Monti, F.E. Gabaly, M.F. Campbell, P.E. Schrader, D.M. Popolan-Vaida, N.K. Richards-Henderson, K.R. Wilson, A. Violi, H.A. Michelsen, Formation and emission of large furans and oxygenated hydrocarbons from flames, Proc. Natl. Acad. Sci. 113 (2016) 8374–8379. https://doi.org/10.1073/pnas.1604772113.

[3] N. Hansen, M. Schenk, K. Moshammer, K. Kohse-Höinghaus, Investigating repetitive reaction pathways for the formation of polycyclic aromatic hydrocarbons in combustion processes, Combust. Flame. 180 (2017) 250–261. https://doi.org/10.1016/j.combustflame.2016.09.013.

[4] M. Nowakowska, O. Herbinet, A. Dufour, P.-A. Glaude, Detailed kinetic study of anisole pyrolysis and oxidation to understand tar formation during biomass combustion and gasification, Combust. Flame. 161 (2014) 1474–1488. https://doi.org/10.1016/j.combustflame.2013.11.024.

[5] X. Li, Y. Zheng, C. Guan, C.S. Cheung, Z. Huang, Effect of biodiesel on PAH, OPAH, and NPAH emissions from a direct injection diesel engine, Environ. Sci. Pollut. Res. 25 (2018) 34131–34138. https://doi.org/10.1007/s11356-018-3382-3.

[6] Q. He, Q. Guo, K. Umeki, L. Ding, F. Wang, G. Yu, Soot formation during biomass gasification: A critical review, Renew. Sustain. Energy Rev. 139 (2021) 110710. https://doi.org/10.1016/j.rser.2021.110710.

[7] I. Abbas, G. Badran, A. Verdin, F. Ledoux, M. Roumié, D. Courcot, G. Garçon, Polycyclic aromatic hydrocarbon derivatives in airborne particulate matter: sources, analysis and toxicity, Environ. Chem. Lett. 16 (2018) 439–475. https://doi.org/10.1007/s10311-017-0697-0.

[8] W. Huang, B. Huang, X. Bi, Q. Lin, M. Liu, Z. Ren, G. Zhang, X. Wang, G. Sheng, J. Fu, Emission of PAHs, NPAHs and OPAHs from residential honeycomb coal briquette combustion, Energy Fuels. 28 (2014) 636–642. https://doi.org/10.1021/ef401901d.

[9] S. Suzuki, S. Kiuchi, K. Kinoshita, Y. Takeda, K. Tanaka, M. Oguma, Formation of Polycyclic Aromatic Hydrocarbons (PAHs) and Oxygenated PAHs in the Oxidation of Ethylene Using a Flow Reactor, Combust. Sci. Technol. 0 (2020) 1–27. https://doi.org/10.1080/00102202.2020.1771327.

[10] S. Suzuki, S. Kiuchi, K. Kinoshita, Y. Takeda, S. Sakaida, M. Konno, K. Tanaka, M. Oguma, Formation of polycyclic aromatic hydrocarbons, benzofuran, and dibenzofuran in fuel-rich oxidation of toluene using a flow reactor, Phys. Chem. Chem. Phys. 23 (2021) 6509–6525. https://doi.org/10.1039/D0CP06615J.

[11] P. Liu, B. Chen, Z. Li, A. Bennett, S. Sioud, S.M. Sarathy, W.L. Roberts, Evolution of oxygenated polycyclic aromatic hydrocarbon chemistry at flame temperatures, Combust. Flame. 209 (2019) 441–451. https://doi.org/10.1016/j.combustflame.2019.08.018.

[12] X. Shi, Q. Wang, A. Violi, Chemical pathways for the formation of benzofuran and dibenzofuran in combustion, Combust. Flame. 212 (2020) 216–233. https://doi.org/10.1016/j.combustflame.2019.10.008.
[13] M. Frenklach, Reaction mechanism of soot formation in flames, Phys. Chem. Chem. Phys. 4 (2002) 2028–2037. https://doi.org/10.1039/B110045A.
[14] M. Altarawneh, B.Z. Dlugogorski, E.M. Kennedy, J.C. Mackie, Quantum Chemical Study of Low Temperature Oxidation Mechanism of Dibenzofuran, J. Phys. Chem. A. 110 (2006) 13560–13567. https://doi.org/10.1021/jp065135r.
[15] M. Keita, A. Nicolle, A.E. Bakali, A wide range kinetic modeling study of PAH formation from liquid transportation fuels combustion, Combust. Flame. 174 (2016) 50–67. https://doi.org/10.1016/j.combustflame.2016.09.016.
[16] T. Bierkandt, P. Hemberger, P. Oßwald, D. Krüger, M. Köhler, T. Kasper, Flame structure of laminar premixed anisole flames investigated by photoionization mass spectrometry and photoelectron spectroscopy, Proc. Combust. Inst. 37 (2019) 1579–1587. https://doi.org/10.1016/j.proci.2018.07.037.
[17] S.W. Wagnon, S. Thion, E.J.K. Nilsson, M. Mehl, Z. Serinyel, K. Zhang, P. Dagaut, A.A. Konnov, G. Dayma, W.J. Pitz, Experimental and modeling studies of a biofuel surrogate compound: laminar burning velocities and jet-stirred reactor measurements of anisole, Combust. Flame. 189 (2018) 325–336. https://doi.org/10.1016/j.combustflame.2017.10.020.
[18] Y. Wu, B. Rossow, V. Modica, X. Yu, L. Wu, F. Grisch, Laminar flame speed of lignocellulosic biomass-derived oxygenates and blends of gasoline/oxygenates, Fuel. 202 (2017) 572–582. https://doi.org/10.1016/j.fuel.2017.04.085.
[19] E. Ranzi, A. Frassoldati, A. Stagni, M. Pelucchi, A. Cuoci, T. Faravelli, Reduced Kinetic Schemes of Complex Reaction Systems: Fossil and Biomass-Derived Transportation Fuels, Int. J. Chem. Kinet. 46 (2014) 512–542.
[20] W. Yuan, T. Li, Y. Li, M. Zeng, Y. Zhang, J. Zou, C. Cao, W. Li, J. Yang, F. Qi, Experimental and kinetic modeling investigation on anisole pyrolysis: Implications on phenoxy and cyclopentadienyl chemistry, Combust. Flame. 201 (2019) 187–199. https://doi.org/10.1016/j.combustflame.2018.12.028.
[21] B. Chen, S. Kruse, R. Schmid, L. Cai, N. Hansen, H. Pitsch, Oxygenated PAH Formation Chemistry Investigation in Anisole Jet Stirred Reactor Oxidation by a Thermodynamic Approach, Energy Fuels. 35 (2021) 1535–1545. https://doi.org/10.1021/acs.energyfuels.0c03829.
[22] B. Shukla, M. Koshi, A novel route for PAH growth in HACA based mechanisms, Combust. Flame. 159 (2012) 3589–3596. https://doi.org/10.1016/j.combustflame.2012.08.007.
[23] M. J. Frisch, G. W. Trucks, H. B. Schlegel, G. E. Scuseria, M. A. Robb, J. R. Cheeseman, G. Scalmani, V. Barone, G. A. Petersson, H. Nakatsuji, X. Li, M. Caricato, A. V. Marenich, J. Bloino, B. G. Janesko, R. Gomperts, B. Mennucci, H. P. Hratchian, J. V. Ortiz, A. F. Izmaylov, J. L. Sonnenberg, Williams, F. Ding, F. Lipparini, F. Egidi, J. Goings, B. Peng, A. Petrone, T. Henderson, D. Ranasinghe, V. G. Zakrzewski, J. Gao, N. Rega, G. Zheng, W. Liang, M. Hada, M. Ehara, K. Toyota, R. Fukuda, J. Hasegawa, M. Ishida, T. Nakajima, Y. Honda, O. Kitao, H. Nakai, T. Vreven, K. Throssell, J. A. Montgomery Jr., J. E. Peralta, F. Ogliaro, M. J. Bearpark, J. J. Heyd, E. N. Brothers, K. N. Kudin, V. N. Staroverov, T. A. Keith, R. Kobayashi, J. Normand, K. Raghavachari, A. P. Rendell, J. C. Burant, S. S. Iyengar, J. Tomasi, M. Cossi, J. M. Millam, M. Klene, C. Adamo, R. Cammi, J. W. Ochterski, R. L. Martin, K. Morokuma, O. Farkas, J. B. Foresman, D. J. Fox, Gaussian 16 Rev. A.03, Wallingford, CT, 2016.
[24] D.O. Kashinski, G.M. Chase, R.G. Nelson, O.E. Di Nallo, A.N. Scales, D.L. VanderLey, E.F.C. Byrd, Harmonic Vibrational Frequencies: Approximate Global Scaling Factors for TPSS, M06, and M11 Functional Families Using Several Common Basis Sets, J. Phys. Chem. A. 121 (2017) 2265–2273. https://doi.org/10.1021/acs.jpca.6b12147.
[25] NIST, http://webbook.nist.gov/chemistry/, 2013. http://webbook.nist.gov/chemistry/.
[26] H.-J. Werner, P.J. Knowles, G. Knizia, F.R. Manby, M. Schütz, P. Celani, W. Györffy, D. Kats, T. Korona, R. Lindh, A. Mitrushenkov, G. Rauhut, K.R. Shamasundar, T.B. Adler, R.D. Amos, S.J.

Bennie, A. Bernhardsson, A. Berning, D.L. Cooper, M.J.O. Deegan, A.J. Dobbyn, F. Eckert, E. Goll, C. Hampel, A. Hesselmann, G. Hetzer, T. Hrenar, G. Jansen, C. Köppl, S.J.R. Lee, Y. Liu, A.W. Lloyd, Q. Ma, R.A. Mata, A.J. May, S.J. McNicholas, W. Meyer, T.F.M. III, M.E. Mura, A. Nicklass, D.P. O'Neill, P. Palmieri, D. Peng, K. Pflüger, R. Pitzer, M. Reiher, T. Shiozaki, H. Stoll, A.J. Stone, R. Tarroni, T. Thorsteinsson, M. Wang, M. Welborn, Molpro, Version 2019.2, 2019.

[27] D.W. Schwenke, The extrapolation of one-electron basis sets in electronic structure calculations: How it should work and how it can be made to work, J. Chem. Phys. 122 (2004) 014107. https://doi.org/10.1063/1.1824880.

[28] J.G. Hill, K.A. Peterson, G. Knizia, H.-J. Werner, Extrapolating MP2 and CCSD explicitly correlated correlation energies to the complete basis set limit with first and second row correlation consistent basis sets, J. Chem. Phys. 131 (2009) 194105. https://doi.org/10.1063/1.3265857.

[29] H. Eyring, The activated complex in chemical reactions, J Chem Phys. 3 (1935) 107–115.

[30] H.S. Johnson, Gas phase reaction rate theory, First Edit, Ronald Press, 1966.

[31] K.J. Laidler, Theories of chemical reaction rates, McGraw-Hill, New York, 1969.

[32] C. Eckart, The Penetration of a Potential Barrier by Electrons, Phys. Rev. 35 (1930) 1303–1309. https://doi.org/10.1103/PhysRev.35.1303.

[33] J.-C. Lizardo-Huerta, B. Sirjean, R. Bounaceur, R. Fournet, Intramolecular effects on the kinetics of unimolecular reactions of β-HOROO˙ and HOQ˙OOH radicals, Phys. Chem. Chem. Phys. 18 (2016) 12231–12251.

[34] D. Evgeny, D. Tais, Dissociation Energies of O−H Bonds of Phenols and Hydroperoxides, in: M. Tadashi (Ed.), Appl. Thermodyn. Biol. Mater. Sci., InTech, 2011. https://doi.org/10.5772/13290.

[35] M.-T. Rayez, J.-C. Rayez, J.-P. Sawerysyn, Ab Initio Studies of the Reactions of Chlorine Atoms with Fluoro- and Chloro-Substituted Methanes, J. Phys. Chem. 98 (1994) 11342–11352. https://doi.org/10.1021/j100095a017.

[36] M. Ng, D.K.W. Mok, E.P.F. Lee, J.M. Dyke, A theoretical study of the mechanism of the atmospherically relevant reaction of chlorine atoms with methyl nitrate, and calculation of the reaction rate coefficients at temperatures relevant to the troposphere, Phys. Chem. Chem. Phys. 17 (2015) 7463–7476. https://doi.org/10.1039/C4CP06007E.

[37] I. Webster, SYNTHESIS AND SPECTROSCOPY OF PAH DIMERS, (24-Jun-20). https://www.ideals.illinois.edu/handle/2142/107690 (accessed October 5, 2021).

[38] S. Sinha, R.K. Rahman, A. Raj, On the role of resonantly stabilized radicals in polycyclic aromatic hydrocarbon (PAH) formation: pyrene and fluoranthene formation from benzyl–indenyl addition, Phys. Chem. Chem. Phys. 19 (2017) 19262–19278. https://doi.org/10.1039/C7CP02539D.

[39] D. Khiri, S. Taamalli, D.Q. Dao, T.-B. Nguyen, L. Gasnot, F. Louis, I. Černušák, A. El Bakali, Thermochemical and kinetic studies of hydrogen abstraction reaction from C16H10 isomers by H atoms, Comput. Theor. Chem. 1201 (2021) 113257. https://doi.org/10.1016/j.comptc.2021.113257.

[40] C.-Y. Lin, M.C. Lin, Thermal decomposition of methyl phenyl ether in shock waves: the kinetics of phenoxy radical reactions, J. Phys. Chem. 90 (1986) 425–431. https://doi.org/10.1021/j100275a014.

[41] E.B. Hemings, G. Bozzano, M. Dente, E. Ranzi, Detailed kinetics of the pyrolysis and oxidation of anisole, Chem. Eng. Trans. 24 (2011) 61–66. https://doi.org/10.3303/CET1124011.

[42] Chemkin-Pro 2019R1, ANSYS: Canonsburg, PA, 2019.

[43] B.R. Giri, T. Bentz, H. Hippler, M. Olzmann, Shock-Tube Study of the Reactions of Hydrogen Atoms with Benzene and Phenyl Radicals, Z. Für Phys. Chem. 223 (2009) 539–549. https://doi.org/10.1524/zpch.2009.6036.

[44] J.H. Kiefer, L.J. Mizerka, M.R. Patel, H.C. Wei, A shock tube investigation of major pathways in the high-temperature pyrolysis of benzene, J. Phys. Chem. 89 (1985) 2013–2019. https://doi.org/10.1021/j100256a043.

[45] D.L. Baulch, C.T. Bowman, C.J. Cobos, R.A. Cox, Th. Just, J.A. Kerr, M.J. Pilling, D. Stocker, J. Troe, W. Tsang, R.W. Walker, J. Warnatz, Evaluated Kinetic Data for Combustion Modeling:

Supplement II, J. Phys. Chem. Ref. Data. 34 (2005) 757–1397. https://doi.org/10.1063/1.1748524.
[46] E. Heckmann, H. Hippler, J. Troe, High-temperature reactions and thermodynamic properties of phenyl radicals, Symp. Int. Combust. 26 (1996) 543–550. https://doi.org/10.1016/S0082-0784(96)80258-X.
[47] J. Park, I.V. Dyakov, M.C. Lin, FTIR and Mass-Spectrometric Measurements of the Rate Constant for the C6H5 + H2 Reaction, J. Phys. Chem. A. 101 (1997) 8839–8843. https://doi.org/10.1021/jp972162w.